Applied Catalysis B: Environmental 123–124 (2012) 265–272

Contents lists available at SciVerse ScienceDirect

Applied Catalysis B: Environmental

journal homepage: www.elsevier.com/locate/apcatb

Co_3O_4 nanocrystals on graphene oxide as a synergistic catalyst for degradation of Orange II in water by advanced oxidation technology based on sulfate radicals

Penghui Shi[a,b], Ruijing Su[a], Fengzhi Wan[a], Mincong Zhu[a,c], Dengxin Li[a,*], Shihong Xu[a]

[a] College of Environment Science and Engineering, Donghua University, Shanghai 201620, PR China
[b] Henan University of Urban Construction, Pingdingshan, Henan 467044, PR China
[c] Department of Chemistry and Environmental Science, Zhangzhou Normal University, Zhangzhou, Fujian 363000, PR China

ARTICLE INFO

Article history:
Received 19 December 2011
Received in revised form 26 April 2012
Accepted 27 April 2012
Available online 5 May 2012

Keywords:
Graphene oxide
Cobalt oxide
Sulfate radical
Advanced oxidation processes
Orange II

ABSTRACT

Graphene oxide and cobalt oxide nanocomposites (Co_3O_4/GO) are fabricated in situ as heterogeneous catalysts by the decomposition of cobalt nitrate through heat and crystal growth of Co_3O_4 on the surface of GO sheets in 1-hexanol solvent. The Co_3O_4/GO catalyst is characterized by X-ray diffraction (XRD), Fourier transform infrared spectroscopy (FT-IR), X-ray photoelectron spectroscopy (XPS), energy dispersive X-ray spectroscopy (EDS), scanning electron microscopy (SEM), and high-resolution transmission electron microscopy (HRTEM). Results show that the Co_3O_4/GO catalysts are large GO sheets decorated homogenously with well-dispersed Co_3O_4 nanoparticles. Although Co_3O_4 or GO alone exhibit little catalytic activity, their hybrid (Co_3O_4/GO) exhibits an unexpectedly high catalytic activity in the degradation of Orange II in water by advanced oxidation technology based on sulfate radicals, and 100% decomposition can be achieved in 6 min. These phenomena suggest a synergistic catalytic activity of Co_3O_4 and GO in the hybrid.

© 2012 Elsevier B.V. All rights reserved.

1. Introduction

Advanced oxidation processes (AOPs) that involve in situ generation of highly reactive radicals, such as $^{\bullet}OH$, $^{\bullet}O_2^-$, $^{\bullet}OOH$ and $SO_4^{-\bullet}$, have emerged as a promising method for degradation of organic pollutants [1–4]. Advanced oxidation technologies based on the generation of sulfate radicals ($SO_4^{-\bullet}$) have emerged over the past years as a promising technique to degrade completely most organic pollutants [2,5,6]. The coupling of transition metal ions, such as Cu^{2+}, Mn^{2+}, Fe^{2+}, and Co^{2+} to peroxymonosulfate (PMS) leads to the accelerated generation of $SO_4^{-\bullet}$ and higher oxidation efficiencies [2,6,7]. The various combinations between the dissolved transition metal ions and oxidants have been evaluated systematically for the generation of active radicals by Anipsitakis et al. [2,5,6]. PMS coupled with Co^{2+} ions is the best combination for the generation of $SO_4^{-\bullet}$ for degrading Orange II. However, the oxidation using cobalt and PMS under a homogeneous system has profound disadvantage in terms of the cobalt leachate. The cobalt leachate is biologically toxic and recognized as a priority metal pollutant. Therefore, the activation of PMS by heterogeneous cobalt sources has recently been paid great attention. So, various cobalt precursors were loaded onto various supports to prepare heterogeneous catalyst. Dionysiou et al. [8–10] studied both the unsupported and supported Co_3O_4 on several common supports (i.e., Al_2O_3, SiO_2, and TiO_2) as heterogeneous activators for PMS to degrade 2,4-dichlorophenol (DCP). Kiwi et al. [11] used a polytetrafluoroethylene flexible film as the support for Co_3O_4 nanoparticles to decompose organic dyes under light irradiation. Chen et al. [4] evaluated the performance of unsupported Co_3O_4 nanoparticles in the degradation of Acid Orange 7. Zhang et al. [12] used cobalt oxide on MgO for the degradation of organic dyes in dilute solutions. Shukla et al. [13] studied cobalt exchanged zeolites for the heterogeneous catalytic oxidation of phenol in the presence of peroxymonosulfate.

Similar to hydrogen peroxide, PMS has been proposed as an oxidant. Cobalt ion was proven as an efficient catalyst for PMS activation to produce sulfate radicals and oxidize organic compounds. In the presence of cobalt ion, PMS breaks up to generate active sulfate radicals, which consequently aid in the oxidation of Orange II. Orange II is a widely used synthetic azo dye. It does not decompose through biological methods, and resists light irradiation and chemical oxidation. It is generally used as a model substrate for the aromatic azo dyes. Therefore, several scholars have studied its degradation. In a homogeneous system, the cobalt ion catalyzed activation of PMS and degradation of Orange II as follow reactions:

$$Co^{2+} + HSO_5^- \rightarrow Co^{3+} + SO_4^{-\bullet} + OH^- \quad (1)$$

$$Co^{3+} + HSO_5^- \rightarrow Co^{2+} + SO_5^{-\bullet} + H^+ \quad (2)$$

$$SO_4^{-\bullet} + H_2O \rightarrow SO_4^{2-} + {}^{\bullet}OH + H^+ \quad (3)$$

* Corresponding author. Tel.: +86 21 6779 2541; fax: +86 21 6779 2522.
E-mail addresses: sph1123@163.com (P. Shi), lidengxin@dhu.edu.cn (D. Li).

0926-3373/$ – see front matter © 2012 Elsevier B.V. All rights reserved.
http://dx.doi.org/10.1016/j.apcatb.2012.04.043

$$SO_4^{\bullet -} + [\text{Orange II}] \rightarrow [\text{Orange II}]^- SO_4^{\bullet -} \xrightarrow{-SO_4^{2-}} {}^{\bullet}[\text{Orange II}]^+ \xrightarrow{\text{several steps}} CO_2 + H_2O \quad (4)$$

$$^{\bullet}OH + [\text{Orange II}] \rightarrow [\text{Orange II}]^- {}^{\bullet}OH \xrightarrow{-SO_4^{-}} {}^{\bullet}[\text{Orange II}]^+ \xrightarrow{\text{several steps}} CO_2 + H_2O \quad (5)$$

Graphene oxide (GO), which can be easily prepared by chemical modification, consists of a hexagonal ring-based carbon network with both sp^2-and sp^3-hybridized carbon atoms [14]. This carbon material has multiple oxygen-containing functional groups, such as hydroxyls and epoxides in the basal plane, and carboxyl groups at plane edges [15–19]. Such surface functionalization leads GO swell readily and disperse in water easily [20–24]. Compared with graphene, GO is hydrophilic and can form strong physical interactions with polymers because of its various oxygen functional groups, including hydroxyls, epoxides, carbonyls, and carboxyls [25]. GO sheets can be intercalated or exfoliated by small molecules or polymers [26,27]. These exfoliated GO sheets possess large surface areas and, thus, may be potential support materials to load several nanocrystals, such as a wide range of metals and oxide, fluorescent molecules, drugs, biomolecules and inorganic nanoparticles [28–44].

The current paper reports on a cobalt oxide supported on GO as an efficient heterogeneous catalyst for activation of PMS, used in the degradation of Orange II in water by advanced oxidation technology based on sulfate radicals. It has been found that the Co_3O_4/GO catalyst is able to completely degrade Orange II in dilute solutions within a very short duration of a few minutes without light irradiation and microwave activation, which indicated that Co_3O_4 nanocrystals on GO is a synergistic catalyst. The current catalyst system is therefore expected to be highly desirable for competing with the conventional non-destructive treatment processes.

2. Experimental

2.1. Materials

Flake graphite (300 mesh, 99.99%) was supplied by Shanghai Yifan Graphite Co. Ltd., China. PMS, available as a triple salt of sulfate commercially known as oxone ($2KHSO_5 \cdot KHSO_4 \cdot K_2SO_4$, 4.5% to 4.9% active oxygen), was obtained from Shanghai Ansin Chemical Co. Ltd. and used as an oxidant. Other reagents including $Co(NO_3)_2 \cdot 6H_2O$, H_2SO_4 (98%), $NaNO_3$, $KMnO_4$, and H_2O_2 (30%) of analytical grade were provided by Sinopharm Chemical Reagent Co. Ltd. (China).

2.2. Preparation of GO

Graphite oxide was initially prepared to obtain GO. Graphite oxide was prepared according to the method reported by Hummers and Offeman [45] from purified natural graphite with a mean particle size of 48 μm. Briefly, 230 mL of concentrated H_2SO_4 (98%) was added into a 2000 mL dry flask containing 5 g of $NaNO_3$ placed in an ice-water bath and stirred until the temperature of the mixed liquor is below 5 °C. Then, 10 g of flake graphite was added into the flask, and the mixture was stirred for 30 min. Potassium permanganate (30 g) was added slowly to the suspension under continuous vigorous stirring. The rate of addition was carefully controlled to keep the reaction temperature below 20 °C, and the process required approximately 2 h. Afterward, the ice bath was replaced by an oil bath, and the mixture was stirred at 35 °C for 2 h. The mixture gradually became pasty as the reaction progressed, and the color turned into light brownish. Then, 460 mL of H_2O was slowly added under vigorous stirring, and the reaction temperature was kept at approximately 98 °C. Then, the temperature of the oil bath was set at 90 °C, and the mixture was continuously stirred for 2 h. Finally, 25 ml of 30% H_2O_2 was slowly added to the mixture, and the high-temperature reaction progressed under continuous stirring for 1 h. The mixture color changed into bright yellow from clay black. The mixture was purified by washing with approximately 2 L HCl (5%), followed by deionized (DI) water for several times until no SO_4^{2-} (tested by $BaCl_2$ solution) and Cl^- (tested by $AgNO_3$ solution) were found in the mixture. The mixture color turned to tawny. After filtration and then drying in vacuo at 60 °C for 24 h, graphite oxide was obtained as a solid. GO was obtained through ultrasound stripping of graphite oxide in water or other dissolvent.

2.3. Preparation of Co_3O_4/GO

GO (50 mg) was dispersed into 30 mL of 1-hexanol with sonication for 3 h. The suspension was centrifuged to wipe off the sediment, and the supernate was stored for further use. Then, 1.25 mmol $Co(NO_3)_2 \cdot 6H_2O$ was dissolved into another 20 mL of 1-hexanol and added into the foregoing supernate. The mixture was magnetically stirred for 2 h and heated to 140 °C under reflux and vigorous magnetic stirring for 12 h. After the system was cooled to room temperature, the suspension was centrifuged, and washed by absolute ethanol several times. Then, all the remaining 1-hexanol solvent and other sundries were removed and dried in a vacuum oven at 60 °C for 24 h. The product was labeled as Co_3O_4/GO. Additionally, Co_3O_4 was synthesized with the same parameters for comparison [46].

2.4. Characterization technique

The structural features and the mineralogy of the graphite, GO and Co_3O_4/GO were studied using X-ray diffraction (XRD) patterns obtained on a RIGAKU XRD instrument, using filtered Cu Kα radiation with accelerating voltage of 40 kV and current of 200 mA. The sample was scanned at 2θ from 5° to 90°.

The changes in the surface chemical bonding and surface composition were characterized by Fourier transform infrared spectroscopy (FT-IR; Bruker, Tensor 27), which were obtained to prove the success of support cobalt oxide on the GO sheets. The test samples were pressed into tablets with KBr.

The atomic composition of the GO and Co_3O_4/GO were detected by X-ray photoelectron spectroscopy (XPS). The XPS spectrum was recorded on a ESCALAB 250 photoelectron spectrometer (Thermo-VG Scientific, USA) with Al Kα (1486.6 eV) as the X-ray source. All XPS spectra were corrected using the C 1s line at 284.6 eV.

The texture, morphology, and semi quantitative analyses of the GO and Co_3O_4/GO were performed using scanning electron microscopy (SEM, JEOL JSM-5600LV) with both secondary and backscatter electrons. The elemental composition was determined using the energy dispersive X-ray spectroscopy (EDS). The EDS (IE300X) analysis was performed at several points in the region and averaged to obtain the representative results.

The nanoscale structures were observed using high-resolution transmission electron microscopy (FE-HRTEM, JEOL JEM-2100F) with an accelerating voltage of 200 kV. The sample was prepared by dispersing a small amount of dry powder in ethanol or water. Then, one droplet of the suspension was dropped on a formvar-carbon-coated, 300 mesh copper TEM grids (Ted Pella) covered with thin amorphous carbon film and allowed to evaporate in air at room temperature.

The BET surface areas were measured by a BET analyzer (BK122T-B, JWGB, China) using the liquid nitrogen adsorption method.

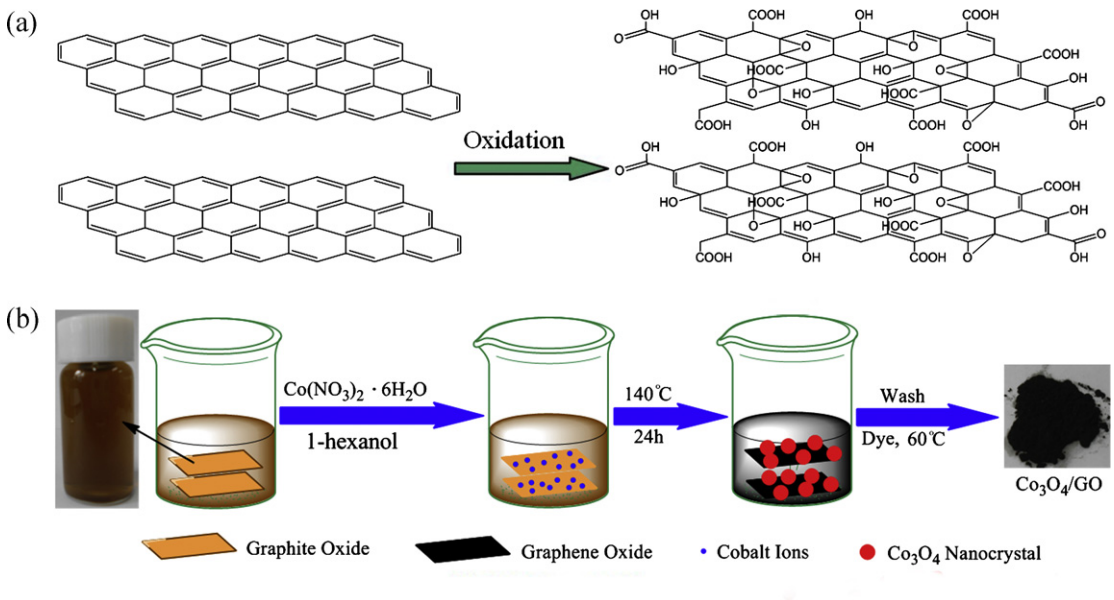

Fig. 1. The schematic of the experimental procedure from graphite to Co_3O_4/GO composite. Graphite to GO (a) and GO to Co_3O_4/GO (b).

The leached Co^{2+} ion concentration was measured by inductively coupled plasma (ICP, Leeman Teledyne) which determines metal ions in a solution for identification and differentiation of metal ions down to ppb levels. Solutions were obtained during the reactions, filtered, and mixed with 2% nitric acid aqueous solution before analysis.

2.5. Evaluation of catalytic activity

The degradation experiments were conducted in a 250 mL vessel. Samples were obtained at regular intervals, joined immediately with $NaNO_2$ (5 g/L) as quencher, and then filtered. Orange II concentration in the filtrate was measured in a UV–vis spectrophotometer (Xinmao 7504) at 486 nm. Co_3O_4/GO (0.1 g/L) and oxone (1 mM) were added in a typical reaction of Orange II degradation with 0.2 mM. Commercial oxone can be used to generate PMS, and 614.7 mg/L (1 mM) of oxone is necessary to release 2 mM PMS. The vessel was placed in a water-bathing constant-temperature vibrator controlled at 25 °C throughout the process. For the purpose of practical application, the additional sulfate ions released by oxone can be reclaimed by ion exchange resin. The addition of PMS led to a significant decrease of pH because PMS is an acidic oxidant. The experiment was conducted both under acidic (pH 2–3, no adjustment) and neutral (pH 7.0, adjusted with 0.5 M phosphate buffer or bicarbonate solution) conditions. For a comparison, the experiment on the catalytic activity of GO and Co_3O_4 in the presence of PMS was conducted in the same conditions.

The catalyst was collected by centrifugation and thoroughly washed with distilled water and ethanol after each recycle during the recycling experiment of the catalyst. Then, the catalyst was dried in a vacuum oven at 60 °C for 24 h to remove water and ethanol. Due to the small particle sizes, catalyst loss was unavoidable during the washing and drying processes. Therefore, several parallel reactions were conducted in the first four runs to ensure that the amount of recycled catalyst was sufficient for the next run. Catalyst dose and other reaction conditions were maintained for the subsequent runs.

3. Results and discussion

3.1. Preparation of composites

A hybrid Co_3O_4/GO composite was obtained through a two-step procedure illustrated in Fig. 1. In the first step, graphite (G) was treated with H_2SO_4 and $KMnO_4$. Graphite oxide that contained a variety of functional groups including carboxyl, hydroxy, epoxy and ketone was obtained (Fig. 1a). In the second step, cobalt ions were coordinated to the surface of graphite oxide. When the graphite oxide dissolved in water or other solvents, its surface formed a number of negative charges. The cobalt ions, which were obtained through the addition of $Co(NO_3)_2{\cdot}6H_2O$, were adsorbed on the surface of graphite oxide using its electrostatic attraction mechanism and in situ formation of Co_3O_4 nanocrystal at 140 °C for 24 h. And the thermogravimetric analysis (TGA) of Co_3O_4/GO indicated a quality score of about 58 wt% for Co_3O_4 in the Co_3O_4/GO material (Supplementary Fig. S2). Several layers of graphite oxide were severed, and GO was formed simultaneously, producing Co_3O_4/GO composites (Fig. 1b). The dominant catalyst particle size was less than 30 μm, which may have exerted certain effects on the catalytic activity. GO is brownish-gray in color and a solid with C:O ratio between 2.1 and 2.9. This material consists of loosely bound layers, each layer being a two-dimensional arrangement of carbon atoms in the graphene pattern with thickness of approximately 1.1 nm [47]. The edges of each layer are terminated with —COOH, —OH, and so on. Thus, GO readily forms a stable aqueous suspension upon ultrasonication and stirring. The oxygen groups on carbon materials can cross-link with TiO_2 [48,49], Fe_3O_4 [28,50], Co_3O_4 [51], and $Fe(OH)_3$ [47]. Thus, treating graphite oxide and hexanol suspension with cobaltous nitrate hexahydrate would generate a composite with cobalt oxide compounds linked on the edge or surface of GO sheets.

3.2. Characterizations of composites

The XRD is an effective method to investigate the interlayer variations and the crystalline properties of the synthesized material. The structural properties of the Co_3O_4/GO were analyzed

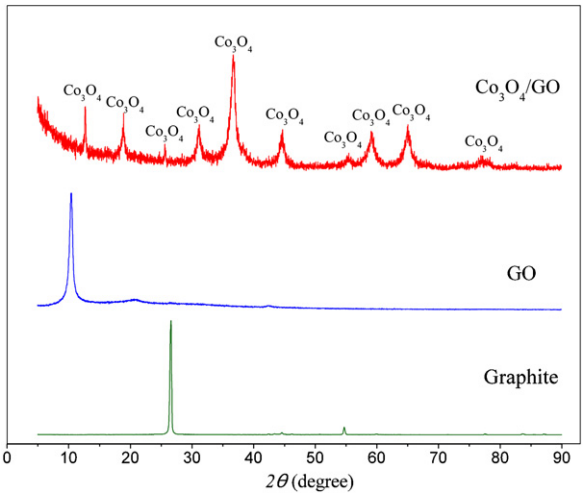

Fig. 2. XRD patterns of graphite (a), GO (b), and Co_3O_4/GO (c).

and compared with those of graphite and GO by XRD (Fig. 2). Graphite showed a very sharp diffraction peak at $2\theta = 26.26^\circ$, corresponding to the interlayer spacing of 0.335 nm. By contrast, the GO pattern showed a characteristic peak at $2\theta = 11.36^\circ$, corresponding to interlayer spacing of 0.78 nm, indicating the presence of oxygen-containing functional groups formed during oxidation. These groups caused the GO sheets to stack more loosely, and the interlayer spacing increased from 0.335 nm to 0.78 nm. The diffraction peak of Co_3O_4/GO was relatively low, indicating that significant face-to-face stacking is absent because of the introduction of Co_3O_4 nanoparticles on both sides of the GO sheets [52]. All the other diffraction peaks can be unambiguously indexed to the Co_3O_4 nanoparticles with a lattice parameter of $a = 8.01$ Å [52]. The relatively weak intensities of the peaks demonstrate the small size of the Co_3O_4 particles. No peaks from other phases have been detected, indicating that the product is of high purity.

The FT-IR spectra of GO and Co_3O_4/GO are presented in Fig. 3 to further support the XRD study. The peaks at 3424 and 1227 cm^{-1} in the IR spectrum of GO (curve a) are attributed to O—H stretching and bending vibration, respectively. The peak at 1722 cm^{-1} corresponds to the stretching band of C=O in carboxylic acid or carbonyl moieties. The other oxygen containing functional groups are revealed by the bands at 1385 and 1076 cm^{-1}, corresponding to epoxide/ether C—O—C and alkoxy or alkoxide C—OH situated at the

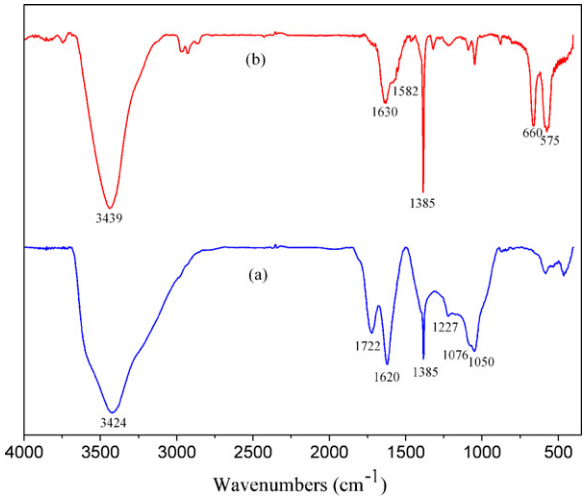

Fig. 3. FT-IR spectra of the original GO (a) and Co_3O_4/GO (b).

edges of GO, respectively [51,53,54]. The deformation of the C—O was observed at 1050 cm^{-1}. The peak at 1620 cm^{-1} (aromatic C=C) can be assigned to the skeletal vibrations of unoxidized graphitic domains. These main characteristic peaks indicate that GO had been synthesized successfully. By contrast, the FT-IR spectra of Co_3O_4/GO (curve b) differed from that of GO as shown by the weakening of the peaks of C=O and O—H at 1630 and 3439 cm^{-1}, respectively. They also showed strong absorptions at 660 and 575 cm^{-1} because of the formation of Co_3O_4, confirming the existence of Co_3O_4. In addition, a new absorption band at approximately 1582 cm^{-1} in the IR spectrum of the residual sediment may be attributed to the skeletal vibration of the GO sheets.

The chemical state of element in GO and Co_3O_4/GO are further provided by XPS measurements (Fig. 4). The binding energies obtained in the XPS analyses were corrected for specimen charging by referencing the C 1s peak to 284.6 eV. The XPS spectra of GO and Co_3O_4/GO composite are illustrated in Fig. 4a. The survey spectra of GO and Co_3O_4/GO shown in Fig. 4a indicates that the XPS spectra of GO have C 1s, O 1s and C 1 2p, whereas the XPS spectra of Co_3O_4/GO exhibit two additional N 1s and Co 2p peaks, in which N originated from the precursor of cobalt nitrate hexahydrate. N-doping of GO may afford stronger coupling between Co and GO in Co_3O_4/GO. N-groups on GO serves as favorable nucleation and anchor sites for Co_3O_4 nanocrystals because of the coordination with Co cations [55]. The N 1s XPS spectrum of Co_3O_4/GO and the C 1s XPS spectrum of GO and Co_3O_4/GO are shown in Fig. 4b and c, respectively. The C 1s XPS spectrum of GO can be deconvoluted into a considerable degree of oxidation with four components that correspond to carbon atoms in different functional groups, as follows: carbon in C—C, C=C, C—H at 284.6 eV; carbon in C—O at 285.2 eV; epoxy carbon at 286.7 eV; and carbonyl carbon (C=O) at 288.1 eV. The C 1s XPS spectrum of the Co_3O_4/GO composite also exhibits the same functionalities, and their peak intensities are a litter smaller than those in GO, indicating that some of the epoxide, hydroxyl, and carboxyl functional groups were removed [55,56]. The Co 2p XPS spectra (Fig. 4d) show two major peaks with binding energies at 780.0 and 796.2 eV, corresponding to Co $2p_{3/2}$ and Co $2p_{1/2}$, respectively, with two shake-up satellite peaks located at approximately 6 eV above the main peaks, which is characteristic of a Co_3O_4 phase and in good agreement with the reported data [52,57,58]. This result is consistent with the XRD and FT-IR analyses.

The typical SEM images (Fig. 5) show the morphology of the synthesized GO and Co_3O_4/GO as well as confirm the presence of Co_3O_4 nanoparticles in the samples. In contrast to the surface of GO which was quite smooth (Fig. 5a), the Co_3O_4 added on GO appeared as bright dots uniformly spread over the surface of GO. The Co_3O_4 spheres were uniformly decorated and firmly anchored on the wrinkled high-density GO layers (Fig. 5b). There was agglomeration of the Co_3O_4 nanoparticles on GO. A homogeneous dispersion of Co_3O_4 nanoparticles in the GO matrix that are eager to accumulate along the wrinkles and edge of visible GO sheets is also revealed in Fig. 5b. The nanoparticles were not simply mixed up or blended with GO. They may have been entrapped inside the GO sheets. However, the EDS (Fig. 6) of Co_3O_4/GO clearly show the presence of cobalt in the sample, and that the sample consisted mainly of cobalt, carbon, and oxygen. EDS analyses on the particle suggest the presence of both cobalt and carbon elements, signifying that the GO particles are completely coated by a layer of cobalt oxide, consistent with FT-IR and SEM morphology.

The TEM images (Fig. 7) can provide better qualitative understanding of the internal structure and spatial distribution, as well as dispersion of GO sheets and Co_3O_4 anchored on the surface of GO, through direct visualization. Most of the GO sheets were dispersed as tactoids with large thicknesses, smooth surfaces, and wrinkled edges (Fig. 7a). A uniform dispersion of Co_3O_4 nanoparticles on the GO sheets is demonstrated in Fig. 7b. Fig. 7c and d shows Co_3O_4

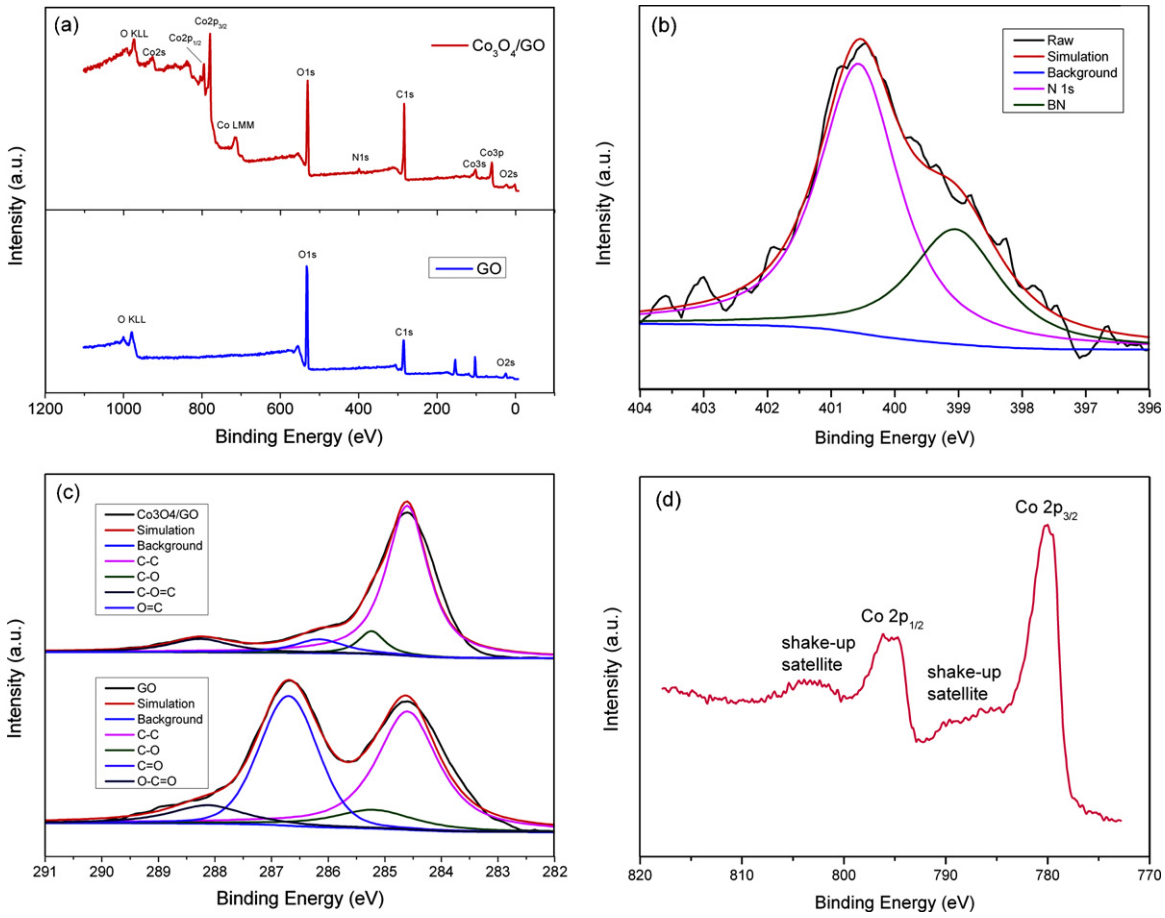

Fig. 4. XPS survey spectra of GO and Co_3O_4/GO (a), N 1s XPS spectra of Co_3O_4/GO (b), C 1s XPS spectra of GO and Co_3O_4/GO, (c) and Co 2p XPS spectra of Co_3O_4/GO.

particles (3 nm to 5 nm in size) are dispersed fairly homogeneously on the surface of GO and the lattice fringes of Co_3O_4 are about 0.191 nm and 0.184 nm. All the images prove that the present catalyst preparation produces large GO sheets homogenously decorated with well-dispersed Co_3O_4 nanoparticles.

3.3. Degradation of Orange II performances

The degradation curves of Orange II under different conditions were shown in Fig. 8. All experiments were conducted in neutral conditions (adjusted with 0.5 M phosphate buffer) with the catalyst (Co_3O_4, GO or Co_3O_4/GO) dosage of 0.1 g/L and the pH during the entire reaction process was almost constant. Curves a, b and c indicated the adsorption of Orange II onto Co_3O_4, GO and Co_3O_4/GO, respectively. The adsorption/desorption was found to be a reversible process, the concentration of Orange II only decreased around 10% in the first few minutes and then a plateau was reached. Since a negligible extent of dye removal occurred without PMS, the small drop in Orange II concentration could be due to the physical adsorption on the Co_3O_4, GO or Co_3O_4/GO surface. In the reaction liquid (with 2 mM PMS and without a catalyst), the degradation occurred very slowly and approximately 47% of Orange II was degraded in the first 60 min (curve d). Curves e, f and g indicate the catalytic activity of GO, Co_3O_4 and Co_3O_4/GO, respectively. Both GO and Co_3O_4 displayed little catalytic activity in the presence of PMS, and there is still 52% and 34% of Orange II remaining

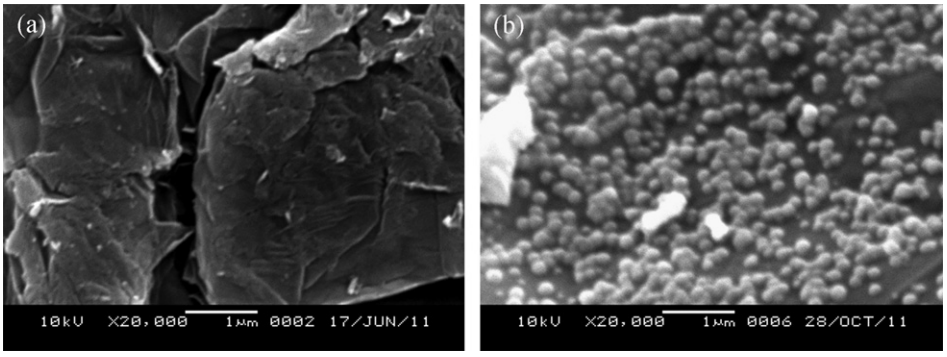

Fig. 5. SEM images of the synthesized GO (a) and Co_3O_4/GO (b).

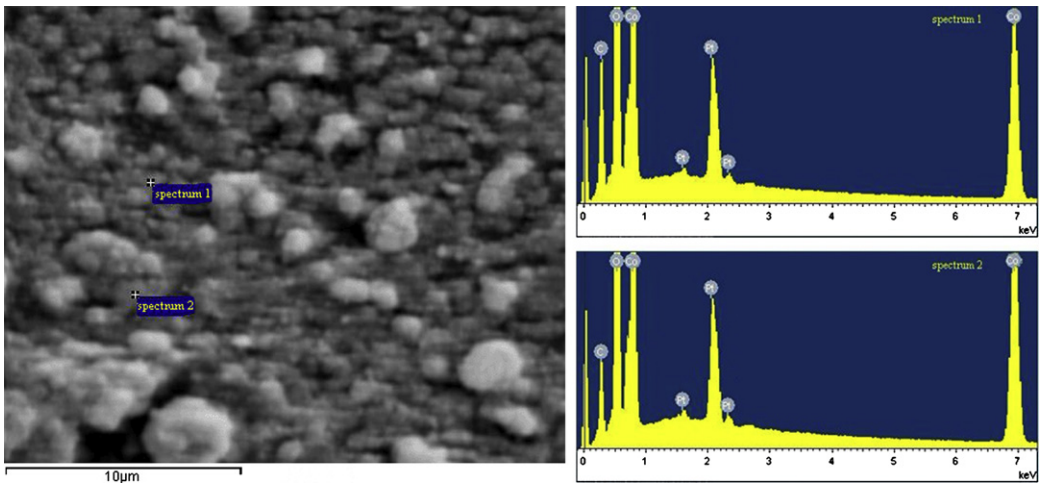

Fig. 6. EDS spectra of the Co_3O_4/GO. The Pt signals come from the plated element.

in the first 30 min. However, the Orange II degradation rate can reach 100% within 6 min using Co_3O_4/GO/PMS system. Therefore, it confirms that the quick decrease of Orange II concentration in the presence of both Co_3O_4/GO and PMS is due to the catalytic destruction of Orange II rather than the non-destructive adsorption of Orange II on the surface of the catalyst. Curve h shows that the homogeneous Co^{2+} ions dissolved from $Co(NO_3)_2$ resulted in the complete degradation of Orange II within 24 min under the same condition. This result was similar to those reported by Chen et al. [4] and Xu et al. [12]. Thus the Co_3O_4/GO catalyst prepared in this work was more active than the homogeneous Co^{2+} ions and the heterogeneous unsupported Co_3O_4 catalyst. Although Co_3O_4 or GO alone has little catalytic activity, their hybrid (Co_3O_4/GO) exhibits an unexpected high catalytic activity in degradation of Orange II in water by advanced oxidation technology based on sulfate radicals. Hence, 100% decomposition can be achieved in 6 min suggesting synergistic coupling between Co_3O_4 and GO is indispensable to the high catalytic activity of the hybrid.

3.4. Heterogeneous activity of Co_3O_4/GO

Cobalt leaching has been paid great attention because of the highly efficient activation of PMS by homogeneous Co^{2+} ions [12]. The previous reports have shown that cobalt leaching from the heterogeneous nano-Co_3O_4, as well as in the supported Co/MgO, Co/TiO_2, and Co/Al_2O_3 catalysts, was usually <1% even in acidic solutions [1,8,10,12,59]. The cobalt concentration leached from the reaction solution after filtration by microfiltration membrane (0.45 μm) was tested by ICP in the current study. The leached cobalt concentration was very low because a low catalyst concentration (10 mg Co_3O_4/GO in 100 mL solution) was used in the reaction. The cobalt leachate testing by ICP is illustrated in Fig. 9. The cobalt leachate is below 0.5 mg/L without any pH adjustment, and the final percentage of Co lost from the material is about 0.5%. While, there was hardly any cobalt leachate under neutral pH. The ICP results indicate that there is no correlation between the activity of the catalyst and the dissolved cobalt ion concentrations, and the activation

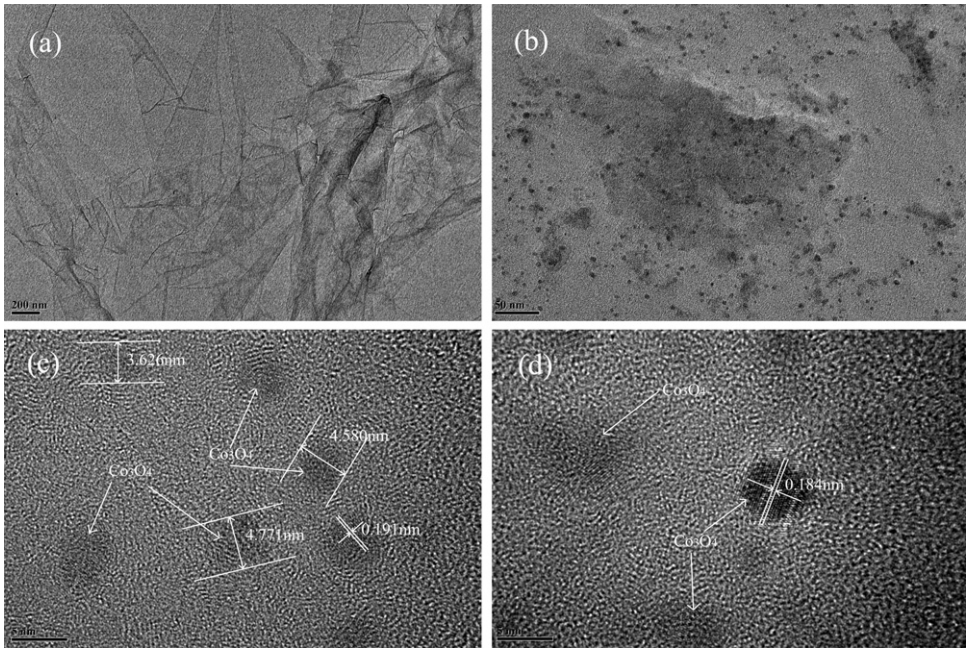

Fig. 7. TEM images of the GO sheets (a) and Co_3O_4/GO with low (b) and high-magnification (c and d).

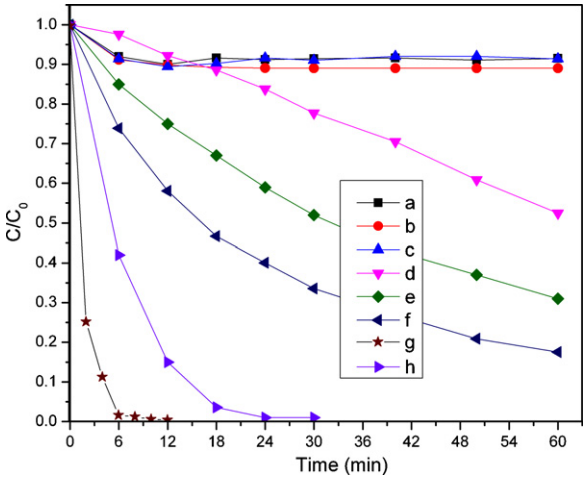

Fig. 8. Degradation curves of Orange II under different conditions: (a) [Co_3O_4] = 0.1 g/L; (b) [GO] = 0.1 g/L; (c) [Co_3O_4/GO] = 0.1 g/L; (d) [PMS] = 2 mM; (e) [GO] = 0.1 g/L and [PMS] = 2 mM; (f) [Co_3O_4] = 0.1 g/L and [PMS] = 2 mM; (g) [Co_3O_4/GO] = 0.1 g/L and [PMS] = 2 mM; (h) [Co^{2+}] = 0.07 g/L and [PMS] = 2 mM.

of PMS by the catalyst is through the heterogeneous pathway. The Co_3O_4 nanoparticles supported on GO are apparently a stable cobalt source to accelerate the generation of sulfate radicals from PMS, and the presence of the GO support leads to much higher acceleration efficiency.

3.5. Stability of Co_3O_4/GO in multiple runs

Five recycling runs of the Co_3O_4/GO were performed, and the catalyst under the same reaction conditions was recycled to evaluate the stability of the Co_3O_4/GO catalyst. The activity of the catalyst dropped slightly compared with the fresh catalyst (Fig. 10). The concentration of dissolved Co ions from Co_3O_4 was almost the same as that in the fresh catalyst as detected by ICP. Meanwhile, the surface area measurement of the fresh and used Co_3O_4/GO after the first cycle via nitrogen gas absorption yielded a BET value of 126.7 m^2/g and 118.4 m^2/g. Therefore, both the amount of Co lost from the catalyst and the reduction of BET value may be responsible for the activity decay. But, the degradation of Orange II after five runs occurred in 12 min similar to the first run. Therefore, Co_3O_4/GO has good catalytic performance and little ion leaching, indicating that the catalyst has excellent long-term stability.

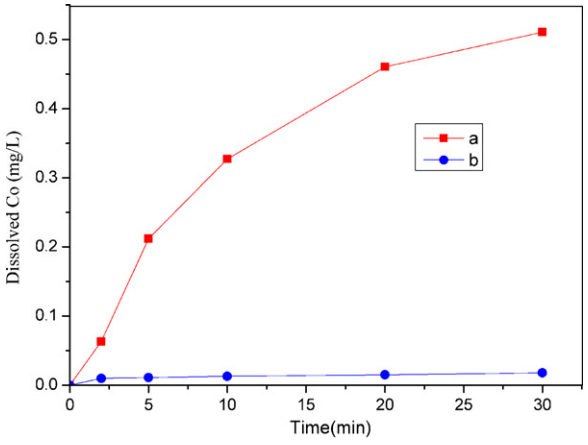

Fig. 9. Dissolution of Co from Co_3O_4/GO under acidic (a) and neutral (b) pH. Conditions: [Orange II]$_0$ = 0.2 mM, [Co_3O_4/GO] = 0.1 g/L, and [PMS] = 2 mM.

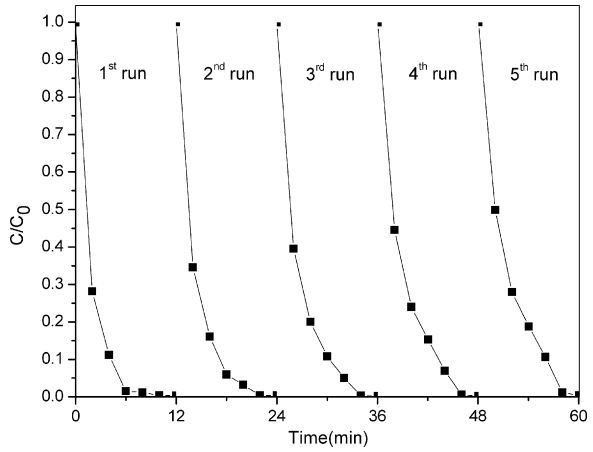

Fig. 10. Degradation of Orange II in consecutive runs using the recycled Co_3O_4/GO catalyst at neutral pH, [Orange II] = 0.2 mM, [Co_3O_4/GO] = 0.1 g/L and [PMS] = 2 mM.

4. Conclusions

A route to prepare Co_3O_4/GO nanocomposites in a solvothermal system is proposed in the current study. The structure of the Co_3O_4/GO is stable, and the well-dispersed nanoscale Co_3O_4 particles (3 nm to 5 nm) on GO indicates a high surface area, excellent structure, and perfect catalytic properties. The supported Co_3O_4/GO catalyst also exhibits a markedly better efficiency for PMS activation than both the homogeneous Co^{2+} and the heterogeneous unsupported Co_3O_4 catalyst. The Co_3O_4/GO exhibits good heterogeneous activity in the degradation of Orange II used in advanced oxidation technology based on sulfate radicals, which can accomplish the degradation of Orange II within 6 min and with little cobalt leachate. Thus, Co_3O_4 nanocrystals on GO is a synergistic catalyst for degradation of Orange II in water by advanced oxidation technology based on sulfate radicals.

Acknowledgments

The study was supported by the Fundamental Research Funds for the Central Universities (12D11319), Innovation Program of Shanghai Municipal Education Commission (12ZZ069), Shanghai Municipal Natural Science Foundation (no. 11ZR1400400), Fundamental Research Funds for the Central Universities (no. 11D11303), Shanghai Leading Academic Discipline Project (no. B604), Henan Provincial Department of Education on Natural Science Foundation Research Programs (2009A610002, 2011A610002) and Henan University of Urban Construction Youth Fund Projects (2010JYB003).

Appendix A. Supplementary data

Supplementary data associated with this article can be found, in the online version, at http://dx.doi.org/10.1016/j.apcatb.2012.04.043.

References

[1] E. Chamarro, A. Marco, S. Esplugas, Water Research 35 (2001) 1047–1051.
[2] G.P. Anipsitakis, D.D. Dionysiou, Environmental Science & Technology 37 (2003) 4790–4797.
[3] M. Cheng, W. Ma, J. Li, Y. Huang, J.C. Zhao, Environmental Science & Technology 38 (2004) 1569–1575.
[4] X.Y. Chen, J.W. Chen, X.L. Qiao, D.G. Wang, X.Y. Cai, Applied Catalysis B 80 (2008) 116–121.
[5] G.P. Anipsitakis, D.D. Dionysiou, Applied Catalysis B 54 (2004) 155–163.
[6] G.P. Anipsitakis, D.D. Dionysiou, Environmental Science & Technology 38 (2004) 3705–3712.
[7] I. Sirés, J.A. Garrido, R.M. Rodríguez, E. Brillas, N. Oturan, M.A. Oturan, Applied Catalysis B 72 (2007) 382–394.

[8] Q.J. Yang, H. Choi, Y.J. Chen, D.D. Dionysiou, Applied Catalysis B 77 (2008) 300–307.
[9] Q.J. Yang, H. Choi, D.D. Dionysiou, Applied Catalysis B 74 (2007) 170–178.
[10] G.P. Anipsitakis, E. Stathatos, D.D. Dionysiou, Journal of Physical Chemistry B 109 (2005) 13052–13055.
[11] P. Raja, M. Bensimon, U. Klehm, P. Albers, D. Laub, L. Kiwi-Minsker, A. Renken, J. Kiwi, Journal of Photochemistry and Photobiology A: Chemistry 187 (2007) 332–338.
[12] W. Zhang, H.L. Tay, S.S. Lim, Y.S. Wang, Z.Y. Zhong, R. Xu, Applied Catalysis B 95 (2010) 93–99.
[13] P. Shukla, S.B. Wang, K. Singh, H.M. Ang, M.O. Tadé, Applied Catalysis B 99 (2010) 163–169.
[14] A. Lerf, H. He, M. Forster, J. Klinowski, Journal of Physical Chemistry B 102 (1998) 4477–4482.
[15] S. Park, R.S. Ruoff, Nature Nanotechnology 29 (2009) 217–224.
[16] K.X. Sheng, Y.X. Xu, C. Li, G.Q. Shi, New Carbon Materials 26 (2011) 9–15.
[17] K. Nakada, M. Fujita, G. Dresselhaus, Physical Review B: Condensed Matter 54 (1996) 17954–17961.
[18] H. He, J. Klinowski, M. Forster, Chemical Physics Letters 287 (1998) 53–56.
[19] S.T. Yang, S. Chen, Y.L. Chang, A.N. Cao, Y.F. Liu, H.F. Wang, Journal of Colloid and Interface Science 359 (2011) 24–29.
[20] S. Stankovich, R. Piner, X. Chen, N. Wu, S.T. Nguyen, R.S. Ruoff, Journal of Materials Chemistry 16 (2006) 155–158.
[21] Y. Si, E.T. Samulski, Nano Letters 8 (2008) 1679–1682.
[22] J.I. Paredes, S. Villar-Rodil, A. Martinez-Alonso, J.M.D. Tascon, Langmuir 24 (2008) 10560–10564.
[23] J.T. Yang, M. Wu, F. Chen, Z.D. Fei, M.Q. Zhong, Journal of Supercritical Fluids 56 (2011) 201–207.
[24] F. Wang, K. Zhang, Journal of Molecular Catalysis A: Chemical 345 (2011) 101–107.
[25] R. Li, C.H. Liu, J. Ma, Carbohydrate Polymers 84 (2011) 631–637.
[26] P.G. Liu, K.C. Gong, P. Xiao, M. Xiao, Journal of Materials Chemistry 10 (2000) 933–935.
[27] Y. Matsuo, K. Tahara, Y. Sugie, Carbon 35 (1997) 113–120.
[28] M.Z. Kassaee, E. Motamedi, M. Majdi, Chemical Engineering Journal 172 (2011) 540–549.
[29] N.A. Frey, S. Peng, K. Cheng, S.H. Sun, Chemical Society Reviews 38 (2009) 2532–2542.
[30] G.M. Scheuermann, L. Rumi, P. Steurer, W. Bannwarth, R.J. Mulhaupt, Journal of American Chemical Society 131 (2009) 8262–8270.
[31] A. Cao, Z. Liu, S. Chu, M. Wu, Z. Ye, Z. Cai, Y. Chang, S. Wang, Q. Gong, Y. Liu, Advanced Materials 21 (2009) 103–106.
[32] G. Goncalves, P. Marques, C.M. Granadeiro, H.I.S. Nogueira, M.K. Singh, J. Gracio, Chemistry of Materials 21 (2009) 4796–4802.
[33] A.H. Lu, E.L. Salabas, F. Schuth, Angewandte Chemie International Edition 46 (2007) 1222–1244.
[34] C. Xu, X. Wang, J.W. Zhu, Journal of Physical Chemistry C 112 (2008) 19841–19845.
[35] R. Pasricha, S. Gupta, A.K. Srivastava, Small 5 (2009) 2253–2259.
[36] P.V. Kamat, The Journal of Physical Chemistry Letters 1 (2010) 520–527.
[37] P.V. Kamat, The Journal of Physical Chemistry Letters 2 (2011) 242–251.
[38] K. Vinodgopal, B. Neppolian, I.V. Lightcap, F. Grieser, M. Ashokkumar, P.V. Kamat, The Journal of Physical Chemistry Letters 1 (2010) 1987–1993.
[39] B. Seger, P.V. Kamat, Journal of Physical Chemistry C 113 (2009) 7990–7995.
[40] C.N.R. Rao, A.K. Sood, R. Voggu, K.S. Subrahmanyam, The Journal of Physical Chemistry Letters 1 (2010) 572–580.
[41] I.V. Lightcap, T.H. Kosel, P.V. Kamat, Nano Letters 10 (2010) 577–583.
[42] G. Williams, B. Seger, P.V. Kamat, ACS Nano 2 (2008) 1487–1491.
[43] G. Williams, P.V. Kamat, Langmuir 25 (2009) 13869–13873.
[44] H. Zhang, X. Lv, Y. Li, Y. Wang, J. Li, ACS Nano 4 (2010) 380–386.
[45] W.S. Hummers, R.E. Offeman, Journal of American Chemical Society 80 (6) (1958), 1339–1339.
[46] T. He, D.R. Chen, X.L. Jiao, Chemistry of Materials 16 (2004) 737–743.
[47] K. Zhang, V. Dwivedi, C.Y. Chi, J.S. Wu, The Journal of Hazardous Materials 182 (2010) 162–168.
[48] T.D. Nguyen-Phan, V.H. Pham, E.W. Shin, H.D. Pham, S. Kim, J.S. Chung, E.J. Kim, S.H. Hur, Chemical Engineering Journal 170 (2011) 226–232.
[49] B. Neppolian, A. Bruno, C.L. Bianchi, M. Ashokkumar, Ultrasonics Sonochemistry 19 (2012) 9–15.
[50] S,Y. Wang, S.P. Jiang, X. Wang, Electrochimica Acta 56 (2011) 3338–3344.
[51] H.W. Wang, Z.A. Hu, Y.Q. Chang, Y.L. Chen, Z.Y. Zhang, Y.Y. Yang, H.Y. Wu, Materials Chemistry and Physics 130 (2011) 672–679.
[52] J. Yan, T. Wei, W.M. Qiao, B. Shao, Q.K. Zhao, L.J. Zhang, Z.J. Fana, Electrochimica Acta 55 (2010) 6973–6978.
[53] Y. Xu, H. Bai, G.W. Lu, C. Li, G.Q. Shi, Journal of American Chemical Society 130 (2008) 5856–5857.
[54] S. Stankovich, R.D. Piner, S.T. Nguyen, R.S. Ruoff, Carbon 44 (2006) 3342–3347.
[55] Y.Y. Liang, Y.G. Li, H.L. Wang, J.G. Zhou, J. Wang, T. Regier, H.J. Dai, Nature Materials 8 (2011) 1–7.
[56] S. Stankovich, D.A. Dikin, R.D. Piner, K.A. Kohlhaas, A. Kleinhammes, Y. Jia, Y. Wu, S.T. Nguyen, R.S. Ruoff, Carbon 45 (2007) 1558–1565.
[57] C.D. Wanger, W.M. Riggs, L.E. Davis, J.F. Moulder, G.E. Muilenberg, Handbook of X-ray Photoelectron Spectroscopy, Perkin-Elmer, Eden Prairie, 1978.
[58] C.C. Li, X.M. Yin, T.H. Wang, H.C. Zeng, Chemistry of Materials 21 (2009) 4984–4992.
[59] X.Y. Chen, X.L. Qiao, D.G. Wang, J. Lin, J.W. Chen, Chemosphere 67 (2007) 802–808.